ISSN: 0975 -8542

Journal of Global Pharma Technology

Available Online at: www.jgpt.co.in

RESEARCH ARTICLE

Evaluation the Effects of Fe_3O_4 Nanoparticles on Biofilm Genes Expression Patterns in *Acinetobacter baumannii* using Quantitative Real-Time Polymerase Chain Reaction Assay

Haider Turky Al-Mousawi[1*], Mohammed I. Al-Taee[2], Adil T. Al-Musawi [3]

College of Biotechnology / University of Al-Qassim Green, Institute of Genetic Engineering and Biotechnology / University of Baghdad, Market Research and Consumer Protection Center, University of Baghdad/Iraq.

***Corresponding Author: Haider Turky Al-Mousawi**

Abstract

We selected *Acinetobacter baumannii* isolate from different clinical sources (wounds, burns, urine, sputum, blood and throat) that ability to produce strong biofilm formation, Nanotechnology technique is used in this study, Synthesis magnetic iron oxide nanoparticles Fe_3O_4 NPs using co-precipitation method and detailed physical-chemical characterization, the results show is very fine crystalline sizes reach to 11±1 nm by XRD ,with mostly spherical in shape and average nanoparticles size at (40- 47) nm by SEM and AFM respectively. The minimum inhibitory concentration (MIC) and sub-MIC test of Fe_3O_4 NPs at concentrations (15.75 to 2000) µg/ml toward *A.baumannii* isolates had been determined using Tube broth method. The best sub-MIC concentration of Fe_3O_4 NPs was 125µg/ml with a significant difference at $p > 0.05$ enhanced bacterial adhesion inhibitory on polystyrene surface of microtiter plates and consequently caused biofilms. The results of investigate gene expression of biofilm formation *CsuE* gene with reference 16SrRNA gene by RT-qPCR technique before and after treatment with Fe_3O_4 NPs show a significant difference at $p > 0.05$ in Cycle threshold (Ct) values for gene expression for *CsuE* gene of the isolates. Therefore these treated enhance a significant difference lowest of expression gene fold value for *CsuE* gene and up-regulated at physiological biofilm, while 16SrRNA gene confirmed as well suitable housekeeping gene because do not appear any variations of expression before and after Fe_3O_4 NPs treated.

Keywords: *Acinetobacter baumannii, Fe_3O_4 NPs, Biofilm Formation, Biofilm gene and gene expression.*

Introduction

Acinetobacter baumannii is one of the most challenging pathogens due to its particular multi-drug resistance (MDR) characteristics. World Health Organization (WHO) has recently selected A.baumannii as priority 1 (critical), highlighting its serious threats to public health [1]. This pathogen is an opportunistic Gram negative bacterium, responsible for a broad range of nosocomial infections that frequently found in patients who are admitted to intensive care units (ICUs), ventilator-associated pneumonia ,urinary tract infection, meningitis, burn infection, wound sepsis and bloodstream infections, the mortality rates can reach 35% [2].During the last two decades, A. baumannii has become a pathogen of increased clinical importance due to its remarkable ability to cause several hospital outbreaks of infections due to (MDR) however, it have been reported worldwide, which is remarkable a "serious" threat level pathogen [3]. Biofilm is one of its important microbial virulence factors, however the ability of bacteria to form a biofilm and colonization of host tissue surfaces are an important step in the development of infection.

It is the structural phenotype of microbial communities attached to the moist solid surfaces enclosed in the self-produced heterogeneous polymeric mixtures mainly composed of extracellular polysaccharides substance (EPS), as playing an important role in cell adhesion on biotic or abiotic and the interactions between cells that leads to increased morbidity and mortality [4]. Within a biofilm, bacteria communicate with each other by production of chemotactic particles

or pheromones, as a key behavior coordination mechanism to regulate gene expression in accordance with population density with signal molecules. The pathways are composed of several main parts, including bacteria populations, signal molecules, protein activators and target genes, which influence biofilm formation [5]. Early studies on the *A.baumannii* showed that pilus production mediated by the Csu usher-chaperone assembly system is required for the initial steps of bacterial attachment on abiotic surfaces, resulting in micro colony formation followed by the full development of biofilm [6].

The operon *CsuA/BABCDE* seems to be widespread among clinical isolates, the demonstrated ability of *A.baumannii* strain to adhere by pili to and to form biofilm on abiotic surfaces depending on the expression of CsuE, which is part of the *CsuA/BABCDE* usher-chaperone pili assembly system [7].The CsuE gene is highly preserved in *A.baumannii* and its absence from non-Acb complex species may explain why these species are not able to persist in the hospital environment [8]. Recently the use of nanotechnology to develop new biomaterials, they are displaying important applications in the field of medicine, which can manipulate suitably for desired applications include high sensitivity biomolecular diagnostics, antimicrobial-antibiofilm activities and therapeutics (magnetic target drug delivery, hyperthermia and magnetic resonance imaging).

That has been proposed for the development of new therapeutic products and effective strategies for prophylaxis and treatment of infections [9]. Nanoparticles, usually ranging in dimension from 1-100 nanometers (nm), have properties unique from their bulk equivalent that related to the decrease in the dimensions of the materials to the atomic level [10]. Iron oxide nanoparticles Fe_3O_4 appears to be more resist to microorganisms and are now widely used as antibacterial and antibiofilm agents due to their remarkable properties, superparamagnetism, size (about 10–20 nm) and possibility of receiving a biocompatible coating [11:12]. The ability of Iron oxide nanoparticles to block bacterial growth is represent in prevention of the glycocalyx formation that was helpful to inhibit bacterial adhesion and following biofilm formation on the medical devices. Furthermore, this metal appears to be more resisting to microorganisms; and is now widely used as antibacterial agent [11].

Materials and Methods

Bacterial Strains

A total of ten strong biofilm formation *A. baumannii* clinical isolates was used in this study, as described and identified previously by (AL-mousawi, 2018) were obtained and selected from the Institute of Genetic Engineering and Biotechnology for Post Graduate Studies/ University of Baghdad-IRAQ, these isolates were recovered from Burns swab, Wounds swab, Sputum swab, Urine, Blood and Throat swab. Routine growth and strain preservation was carried out in Luria-Bertani broth (LB) for expression experiments.

Iron Oxide Nanoparticles

Synthesis of the Fe_3O_4 Magnetic Iron Oxide Nanoparticles

The synthesis of Iron oxide nanoparticles Fe_3O_4 NPs were prepared by the co-precipitation method described by [13] with modification. Experimental procedure chemicals used in this study were ferric chloride $FeCl_3.6H_2O$, ferrous sulfate $FeSO_4.7H_2O$, sodium hydrochloride HCl and sodium hydroxide NaOH. All the materials used were analytical grade. The iron salts solution was prepared 3.24 g 0.02 moles of FeCl3.6H2O and 1.99 g 0.01 moles of FeSO4.7H2O provided individually and transferred into a round bottom flask equipped and dissolving in 50 ml of 0.5M HCl solution with a mechanical stirrer magnetic stirrer at 25°C for 20 minutes.

HCl was added to the iron II and III solutions to prevent the initial formation of iron hydroxides. To precipitate magnetite nanoparticles, iron salts solution was dropped into the NaOH alkaline solution 4.58 g of NaOH was added to 14 mL of de-ionized water for 45 minutes at 80°C under a constant stirring speed of 500rpm.

After synthesis by a black gelatinoids appeared, to obtained co-precipitated the particles were separated and collected by an external magnetic field and was repeatedly washed 3 times with deionized water to remove the NaCl, until the supernatant neutral.

The finally, the precipitant was dried under controlled conditions at 50°C for 4 hours and then overnight at room temperature.

Characterization Measurements of Magnetic Iron Oxide Nanoparticles

Structural and optical properties to diagnose Fe_3O_4 NPs have been investigated in this study by various devices were carried out of some measurements are the fallowing technique.

UV-Visible Absorption Spectroscopy

Investigate the optical Absorbance spectra of the Fe_3O_4NPs solution were measured by a double-beam UV-VIS spectrophotometer model (Shimadzu-1). The wavelength range was recorded within the spectral from 295-800 nm [14].

Fourier Transform Infrared (FTIR) Spectroscopy Analysis

Fourier transform infrared spectroscopy was recorded on (FTIR, 8000 Series, Shimadzu) was a useful to investigate the various functional groups present in Fe_3O_4 NPs [15].The spectral rang of iron oxide nanoparticles was record from wavelength range of numbers 400- 4000 cm-1.

X-Ray Diffraction Spectrum (XRD) Technique

X-Ray diffraction device type (XRD, 6000-Shimadzu X-ray Diffract meter) measurements to investigate the crystal structure (crystal phases and to determine the crystallite size of phase of iron oxide nanoparticles [16].The grains size was calculated from the width of the XRD peaks, was used to determine the crystallite size using, Scherer's, equation [17]:

D =, k λ/, ß cos θ..... (1)

Atomic, Force Microscopy, (AFM)

Atomic Force Spectroscopy system model (AFM, AA-3000, USA) was used to characterized the size, surface, roughness, granularity volume distribution and topography of Fe_3O_4 NPs [18].

Scanning Electron Microscopy (SEM) Analysis

Scanning Electron Microscope, type (Inspect S50. fei company Easy Probe Tescan (Netherlands) is generally used to characterize the morphology properties, microstructure of materials (such as crystal structure, particle shape and size) of Fe_3O_4 NPs [19].

Determination of Minimum Inhibitory Concentration (MIC) of Iron Oxide nanoparticles Fe_3O_4 NPs by Tube Method (TM)

The minimum inhibitory concentrations (MIC) of Fe_3O_4 NPs were determined by a method recommended in [20] with some modifications. Briefly: *A.baumannii* isolates was cultured in nutrient agar for overnight. The sterile tubes were used each tube contains 9 ml of bacterial suspension in trypticase soy broth (TSB) with 1% glucose approximate 1.5 ×108 cfu/ml . Then take 1 ml from each of Fe3O4 NPs concentrations (15.75, 31.25, 62.5, 125, 250, 500, 1000 and 2000) µg/ml after introduced to the ultrasound bath apparatus to ensure that the nanoparticles did not agglomerate, was mixed with 9 ml of bacterial growth, then incubated aerobically in shaker incubator for 24 h at 37°C.

The bacterial growth in each tube was measured with spectrophotometer by optical density at 630 nm wavelength. The mean values of inhibition were calculated from triple reading in each test. A broth tube with only bacteria isolates without iron oxides NPs was used as control. MIC was read as the lowest concentration of iron oxide nanoparticles at which there is tube without visible growth of the bacterial cells [21].

Effects of sub-MIC Concentrations of Iron Oxide nanoparticles on biofilm Formation Using Micro titer Plate Method [22]

Overnight *A.baumannii* isolates culture was grown in brain heart infusion broth. Take 100 µl of bacterial suspension approximate 1.5 ×108 cfu/ml was added to the sterile polystyrene microtiter plate with 96 well falt-bottom together with 100 µl of different concentration of Fe_3O_4 NPs, (125) µg/ml in each wells after introduced to the ultrasound bath apparatus to ensure that the nanoparticles did not agglomerate. The control wells contained 180 µl of brain heart infusion broth, and 20 µl of bacterial suspension. Then the culture plates were sealed with para film and were incubated aerobically for 24 h at 37°C.

Then non attached bacterial cells were removed and washing the wells and three times with 200 µl of PBS (pH 7.2). After drying at room temperature, 200 µl of crystal violet (0.1%) added to the wells to stained the biofilms which remained adherent to the walls, then incubation for 10 min. The stained attached bacterial cells were rinsed three times with PBS (pH 7.2).

Then plates were dried properly at room temperature then adding 200 µl of the destaining solution (95% ethanol) for 10 min. The controls were performed with crystal violet binding to the wells exposed only to the culture medium without bacteria. Then, the microtiter plate were measured the values of OD absorbance at 630 nm. Fe_3O_4 NPs effects on biofilm by values of optical density (OD) at 630 nm were determined using ELISA Reader [23]. The inhibition of biofilm formation percentages of iron oxide nanoparticles for each bacterial isolates was calculated as formal described by [24].

Inhibition efficiency (%) = ((Control OD- test OD)/(Control OD)) ×100% …… (2)

The microtiter plate antibiofilim assay estimates the percentage of bacterial biofilm reduction, in relative to the control wells, which were set at 100% to indicate the absence of Fe_3O_4 NPs. In contrast, negative percentage results indicate no inhibition activity of iron oxide nanoparticles on biofilm organization. 2.5. Nuclic acid RNA extraction and relative quantitative real-time PCR of *CsuE* gene Total RNA was extracted from isolated colonies for all A.baumannii isolates from different sources that giving strong biofilm formation was done before treatment with the iron oxide nanoparticles, extract with an DONGSHENG BIOTECH General RNA Extraction kit (Korea) according the manufacturer's recommendations steps.

The RNA concentrations were determined by using NanoDrop Lite Spectrophotometer. Then The RNA was used as a template from which to synthesise cDNA. This standard protocol applies to a single reaction where only template, and water need to be added to the RT FDmix, and the programs used according the manufacturer's recommended. After the PCR program, the synthesis cDNA samples were separated by electrophoresis to shows the band intensity was quantified. Quantification of specific *CsuE* gene F 5′-TAG CGG GCC TGA TGG CAA TT-3′, R 5′-ACC CAG GGC TCT CAA AGA AG-3′ (184 bp) (25) and the reference gene 16SrRNA F 5′- CAG CTC GTG TCG TGA GAT GT -3, R 5′- CGT AAG GGC CAT GAT GAC TT -3′ (150 bp) (26) was used as a control was performed using the real-time PCR in the CFX-96 Thermal Cycler (BioRad Laboratories, Hercules, CA, USA), by using WizOureTM qPCR Master (SYPER) 1-Step RT-qPCR System. This standard protocol applies to single reaction where only template primers, and water need to be added to the qPCR Master (SYPER) and ROD Dye, with the following cycle profile: Initial Denaturation 1 cycle at 95 °C for 5 min followed by 40 cycles at 95 °C for 15 s Denaturation and annealing at 57 °C for 1 min, finally Melting curve analysis 1 cycle at 95 °C for 5 s. The data results of qRT-PCR calculate as it is a direct comparison of threshold cycles (Ct) values between for target and reference (housekeeping) genes were analyzed by the relative quantification gene expression levels (fold change) analysis and one melting curve cycle were analyzed and optimized the ΔΔCt method using software that described by [27]. The PCR amplification as following equations:

ΔCt= Ct target – Ct reference gene…. (3)

ΔΔCt = (Ct target – Ct reference) sample – (Ct target – Ct reference) Calibrator ... (4)

Fold change = 2-ΔΔCT …….. (5)

So, the relative expression changes in mRNA expression levels were determined using comparative threshold cycle (CT) value method (2-ΔΔCt) between the iron oxide nanoparticles treated and untreated for *A. baumannii* isolates.

After Adding the Iron Oxide Nanoparticles Fe_3O_4 NPs on *CsuE* Expression

Relative quantitative real-time PCR (rqRT-PCR) was performed to compare the effect of iron oxide nanoparticles Fe_3O_4 NPs at appropriate concentration on *CsuE* expression gene. Briefly, Lauria Bertini broth tubes 1 × 108 CFU/mL of bacterial cells were inoculated into concentrations of (125) µg/ml of Fe_3O_4 NPs and incubated for 24 hrs at 37 °C. After that, RNA extraction was done by the same steps by DONGSHENG BIOTECH General RNA Extraction kit. Use same genes, RT master mix and programs that used before add Fe_3O_4 NPs, and compare the number of isolates that overexpressed *CsuE* gene.

Statistical Analysis

The results data were analyzed by using Statistical analysis system by using computer program (SPSS), analysis of variance (ANOVA) were used, the level of probability at P values below of ≤ 0.05 that used to identify a significant difference [28].

Results and Discussion

Synthesis of Magnetic Iron Oxide Nanoparticles Fe_3O_4 NPs

The result indicated successfully synthesizing of magnetic iron oxide nanoparticles Fe_3O_4 NPs and show a dark black color with ferromagnetic properties and agreement with [29] them synthesis iron oxide nanoparticles by chemical method.

Characterization of Synthesized Iron Oxide Nanoparticles Fe_3O_4 NPs

UV-Vis Spectroscopy Assay

The UV-Visible absorption spectrum were recorded in the wavelengths ranging region from (290 to 1100 nm) were examined to detect the property of the synthesized iron oxide nanoparticles prepared by precipitation method Figure (3-1). The results showed that the a single peak of the iron oxide nanoparticles were centered exhibit strong surface plasmon resonance absorption below was recorded at approximately 402 nm, while the absorption edge lies between 312 and 750 nm, indicate the formation and the presence of Fe_3O_4 NPs.

Various reports have established that the resonance peak of Fe_3O_4 NPs appears around this region, but the correct position depends on a numeral of factors such as particles size, and the surface adsorbed species [30].

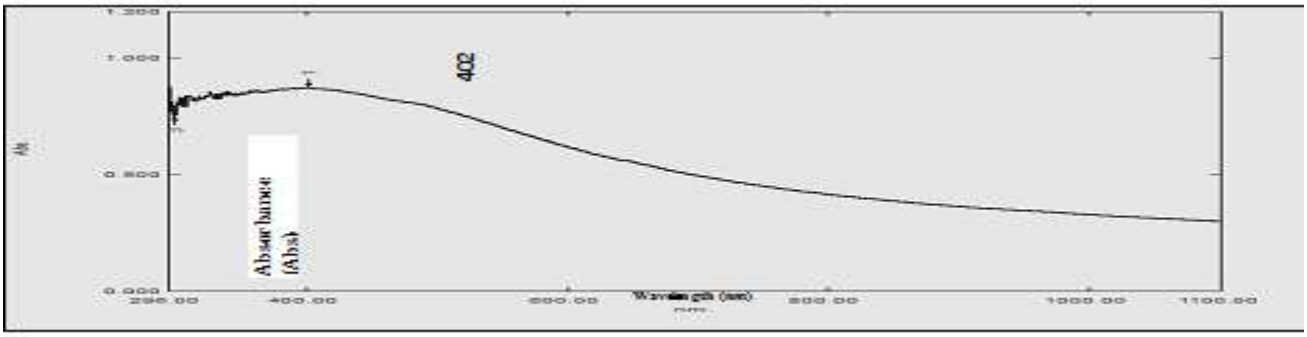

Figure 3-1: UV-Visible spectral analysis of synthesized iron oxide Nanoparticles (Fe3O4 NPs) recorded maximum absorbance at 402nm

Fourier Transform Infrared Spectrum (FTIR) Analysis

The results obtained by FTIR spectroscopy was presented in Figure (3-2) shows the FTIR spectrum of Fe_3O_4 NPs prepared with absorption peaks located in the region of 4000 cm−1 to 400 cm−1, by strong bands at (3415.70, 2362.64, 1633.59, 1433.01, 1008.70, 630.68, 580.53, 567.03 and 451.31) cm-1, corresponds assigned to (hydroxyl group -OH-free, (CH) groups, carbonyl (–C=O) group, phenolic compounds, (COO-) stretching, (C-O) stretch and (C-H) stretching of phenyl ring). The presence of magnetite iron oxide nanoparticles can be seen by three strong absorption bands at peaks 580.53, 567.03 and 451.31 cm-1, which, corresponding to the Fe-O stretching band of bulk magnetite Fe_3O_4. The band locations and amounts of absorption peaks are dependent on chemical composition, crystalline structure and also on morphology [31].

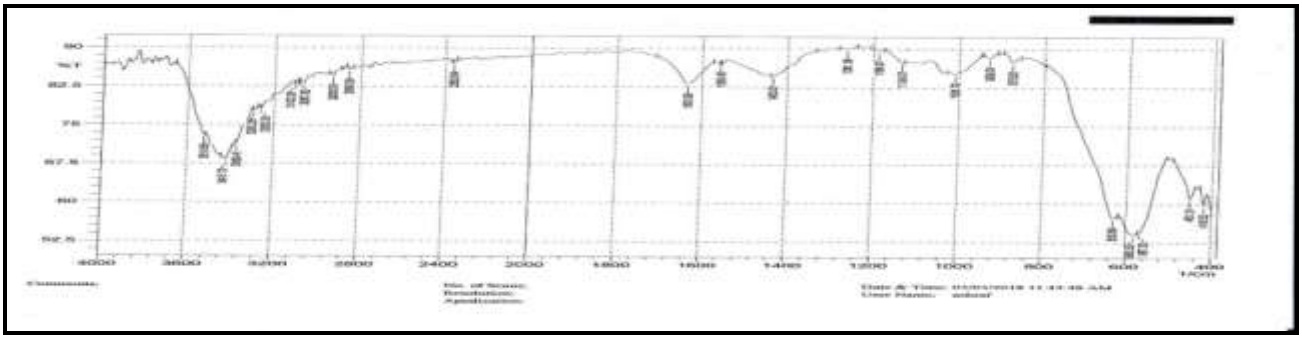

Figure3-2: FTIR spectra pattern of dried powder of synthesized iron oxide Nanoparticles (Fe3O4 NPs)

X-Ray Diffraction Pattern Measurement (XRD)

The result of XRD it is found that there exist eight strong different diffraction peaks corresponding to the crystal planes of crystalline Fe_3O_4 NPs were observed at 2θ (θ=diffraction angle) values of 30.18°, 35.56°, 43.22°, 53.64°, 57.21°, 62.81°, 70.93° and 74.22°, corresponding to the crystalline distance (d) of (2.95), (2.52), (2.09), (1.70), (1.60), (1.47), (1.32) and (1.27) Figure (3-3) Bragg reflection, of crystalline Fe_3O_4 NPs respectively. Indicating the black colored magnetic powders are magnetite nanoparticles with spinel phase structure of magnetite. The average crystallite size of the synthesized Fe_3O_4 NPs in present study can be estimated according to the Debye-Scherrer's equation was found to be in the range of (11±1) nm, which gives a correlation between particle size and peak broadening in XRD, that indicated the synthesis magnetic iron oxide nanoparticles is very fine. The Sharp peaks also suggest that the Fe_3O_4 NPs have good crystallinity and purity structure. Peak broadening observed is consistent with the small particle size [32].

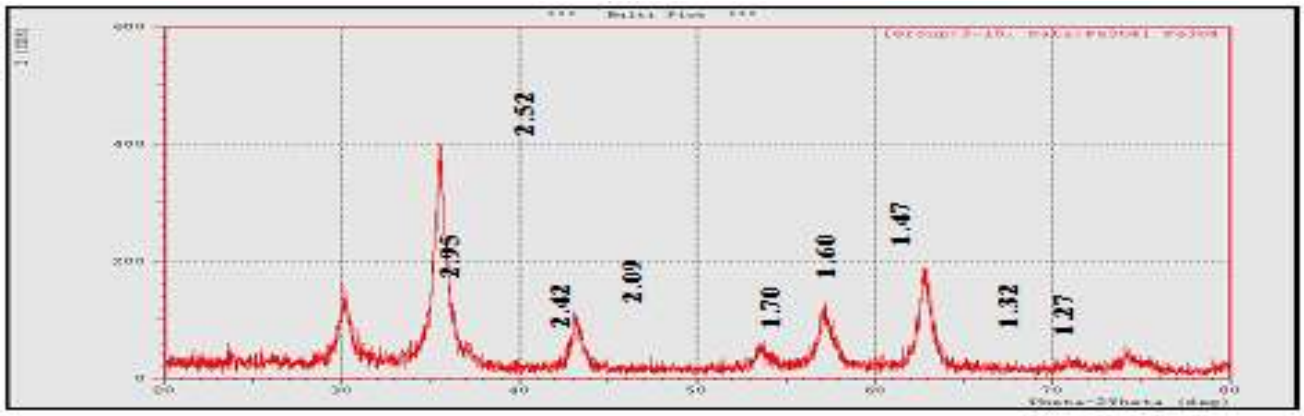

Figure 3-3: X-ray diffraction pattern of synthesized iron oxide Nanoparticles (Fe3O4 NPs)

Atomic Force Microscope (AFM) Analyses

The images of AFM demonstrate an smart interaction among iron oxide nanoparticles leading to the formation of well discrete aggregates. Figure (3-4 A, B) shows a three-dimensional (3D) and two-dimensional (2D) image of a section of the surface of the Fe_3O_4 NPs, where the high molecular clusters which is up 14.93 nm. The average of diameters and sizes composite of Fe_3O_4 NPs that demonstrate in numerous peaks, the highly peaks is (39) from (8-90) nm. Thus the rate of particles sizes (means of average particle size) of the Fe_3O_4 NPs is 47 nm that shown in Figure (3-4 C). It is indicating that the Fe_3O_4 NPs synthesis is manufacturing infinitesimal and uniformly arranged. As the nanoparticles aggregates undergo a brownian action in suspension, scanning in liquid cannot be used for nanoparticle sizing. Sample preparation is vital in order to get useful AFM images. Samples must be thin enough and must hold fast well to the surface, otherwise the scanning method will producing artifacts [33].

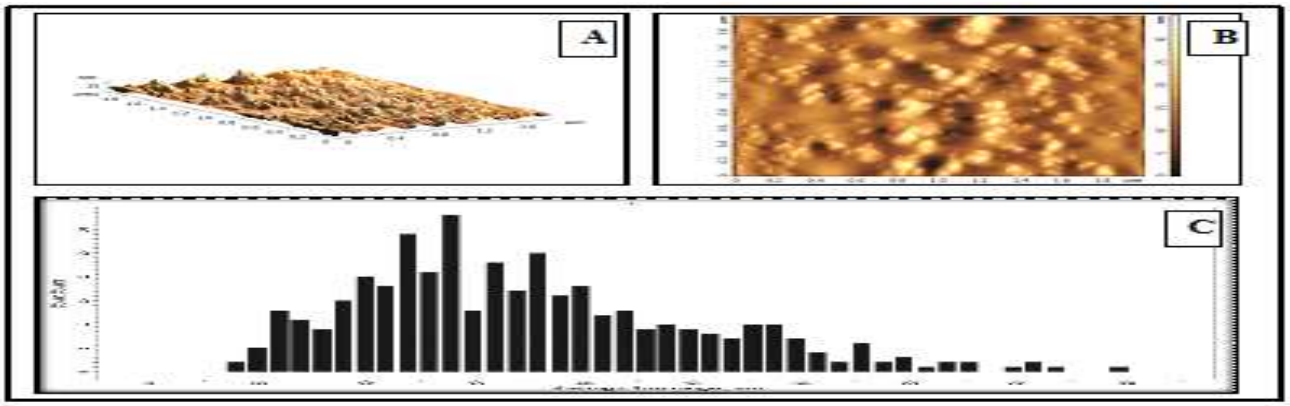

Figure 3-4: Granularity volume distribution chart Image of the synthesized iron oxide nanoparticles (Fe_3O_4 NPs) by Atomic Force Microscope topographic images (A) Three-Dimensional, (B) Two-Dimensional and (C) Average particle size

Field Emission Scanning Electron Microscope (FE-SEM)

SEM images it is evident that the sample consists of by a number quantity of the nanoparticles exhibit spherical shape Fe_3O_4 nanostructures. The average size of the obtained sample approximately 40 nm, indicating that homogeneous magnetite nanoparticles can be synthesized and rather good size distribution. The crystallites of magnetite particles are less agglomerated shown in Figure (3-5).

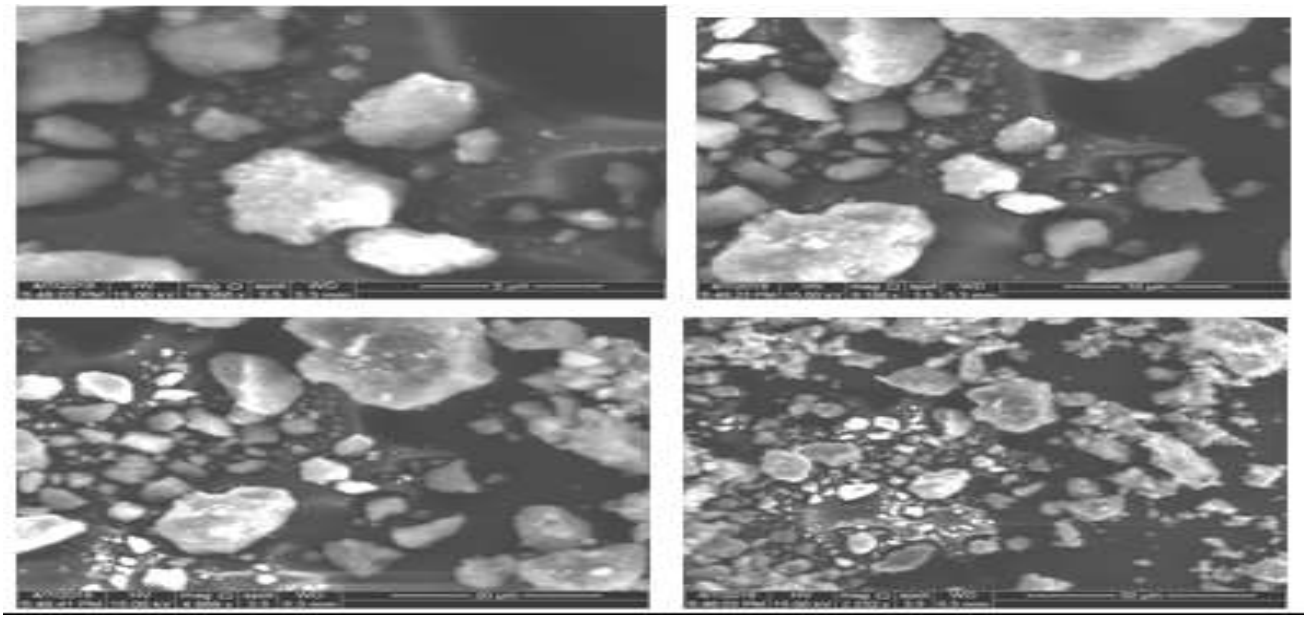

Figure 3-5: Scanning Electron Microscopy (SEM) images (5, 10, 20 and 50) µm of synthesized iron oxide Nanoparticles (Fe3O4 NPs)

Determination the Minimum Inhibitory Concentration (MIC) Test Results for Fe_3O_4 Nanoparticles

The result MIC of Fe3O4 NPs for the antibacterial activities in Tube method was presented in Figure (3-6), shows the optical density (OD) at 630 nm of the means for each concentrations of A.baumannii isolates under study, bacterial culture growth in the presence of Fe_3O_4 NPs by Tube broth medium method compare with OD of the control without NPs. The result showed that the a significant ($p<0.05$) between concentrations (15.75, 31.25, 62.5, 125, 250, 500, 1000 and 2000) µg /ml of synthesis Fe_3O_4 NPs that used are demonstrated different result, the lowest concentration give an inhibition the number of cells of 125 µg /ml concentration, therefore was the best-used concentration of Fe_3O_4 NPs for inhibiting growth of *A.baumannii* isolates. The mode action of the Fe_3O_4 nanoparticles materials were interpreted in terms of the following series process: adsorption onto the bacterial cell surface, diffusion through the cell wall, binding to the cytoplasmic membrane and release of cytoplasmic constituent such as K+ ion, DNA, RNA, and death of the cell [34].

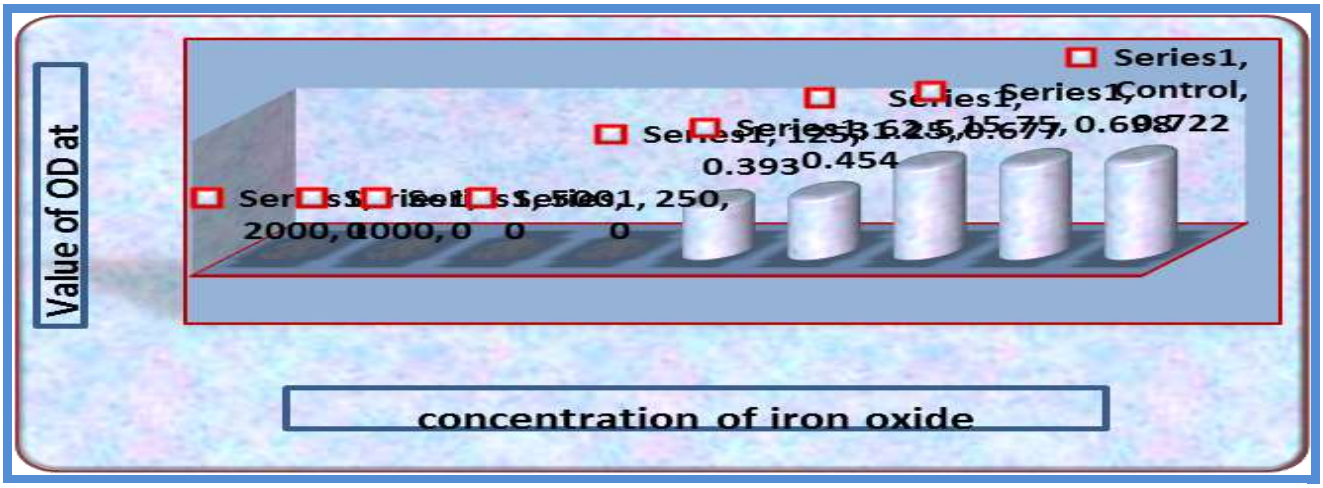

Figure 3-6: Effects of of iron oxide Nanoparticles synthesized (Fe3O4 NPs) on values of OD at 630 nm of *A.baumannii*

The Effect of Sub-MIC of Iron Oxide Nanoparticles Fe_3O_4 NPs on Antibiofilm by Microtiterplate Method

The results showed that the sub-MIC of Fe_3O_4 NPs was 125 µg /ml concentration exhibited a significant reduction in biofilm growth against all *A.baumannii* isolates by the absorbance values was decreased for all isolates after a treatment with sub-MIC of these Fe_3O_4 NPs, with different thickness degrees the absorbance values compared with absorbance values of control that untreated with Fe_3O_4 NPs Figure (3-7). These results indicated that there is a significant difference on biofilm formation after treatment with sub MIC of Fe_3O_4 NPs. The sub-MIC of Fe_3O_4 NPs inhibited bacterial adhesion on polystyrene surface and consequently causes biofilms detachment and this causes decreased in absorbance values of biofilms [35]. Many studies have shown the size dependent antimicrobial and anti-biofilm effects of these nanoparticles and their physico-chemical properties. The small sizes of nanoparticles enables those to penetrate the biofilm matrix and have a high surface to volume ratio, which promotes effective interactions with bacteria and to make contact with bacterial cells cause inhibition of biofilm Furthermore the Fe_3O_4 NPs inhibited biofilm production by blocking the formation of exopolysachrides [36].

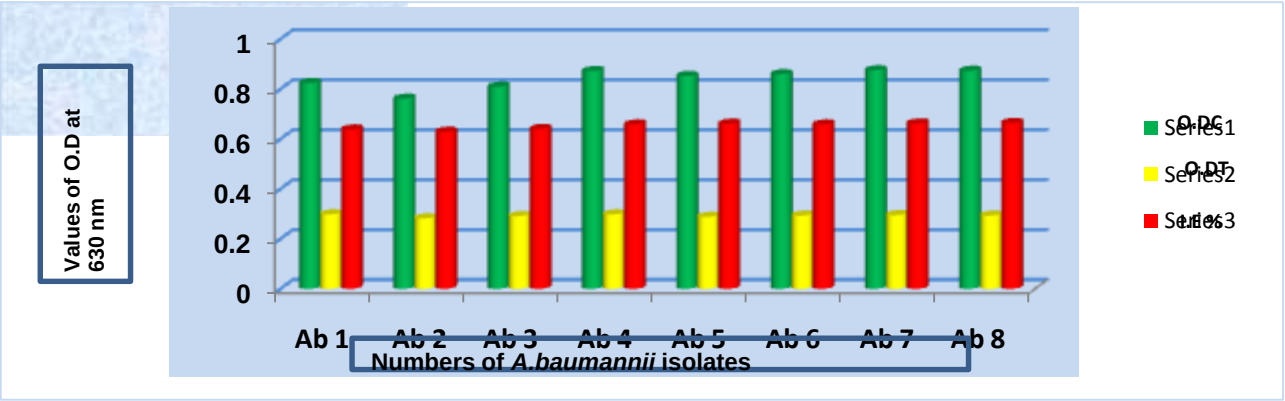

Figure 3-7: biofilm inhibition activity of synthesized iron oxide nanoparticles (Fe3O4 NPs) against *A.baumannii* isolates

Gene Expression Analysis by using qRT PCR Technique

Total RNA and Complementary DNA (cDNA) Reverse Transcription

Before and after treatment with synthetic Fe3O4 NPs, total RNA was carefully extracted by using commercially available RNA extraction for A.baumannii isolates. The concentration of total RNA samples 260/280 ratios should be ranged between from (80 to 220) ng/ µl. The quality and purity of total RNA samples ranged between from (1.79 to 2.19) ng/µl, this was measured using Nanodrop ND-2000 spectrophotometer. cDNA reverse transcription was conducted in the same day of RNA extraction, the efficiency of synthesized cDNA concentration was evaluated through gel electrophoresis to identified cDNA band before real time application Figure (3-8).

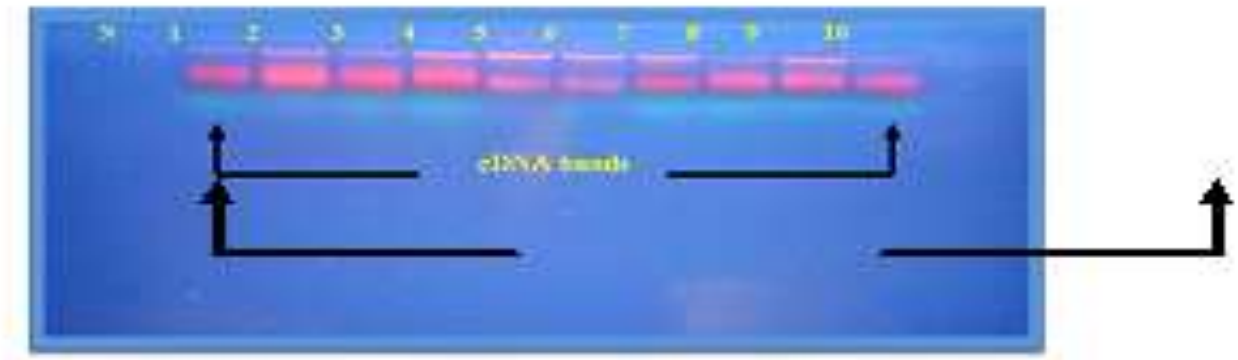

Figure 3-8: Gel electrophoresis detected cDNA bands from *A.baumannii* isolates (1% agarose, 75V, for 30 min stained with ethidium bromide). Lane 1-10: cDNA. Lane N: Negative control (water)

Real time PCR Quantification of *CsuE* gene Expression

In the present study, quantitative RT-PCR assay analyzed the mRNA expression of *CsuE* gene showed significant variation in gene expression biofilm formation for *A.baumannii* isolates. The cycle threshold Ct values of *CsuE* gene amplification were recorded from the software of qRT-PCR, the statistical analysis shown significant differences at values P<0.05 the range from (14.16 to 22.13) before treatment with synthesized Fe_3O_4 NPs. The pattern of amplification of the gene shown in Figures (3-9 A and B) respectively, these variation submit to differences of the sources of isolates. After treatment with Fe_3O_4 NPs by using the concentration below the dose of sub MIC for each sample, the range of Ct value for *CsuE* gene from (17.02 to 24.20), there were significant difference according to LSD values at P<0.05 was found between isolates, the pattern of amplification of this gene showed in Figures (3-9 C and D). The melting curve that show in Figures generated at the end of the PCR reaction show that all amplicon of the *CsuE* gene, this result indicates that no primer–dimmers were formed during the reactions. The statistical analysis also appeared significant differences at values P<0.05 in Ct value where comparing between treated and untreated with Fe_3O_4 NPs for each isolates. Expression of the CsuE gene was decreased in all isolates that treated with Fe_3O_4 NPs, the latter has Ct values were highest than Ct values in untreated, this means decrease gene expression with the increased of Ct values.

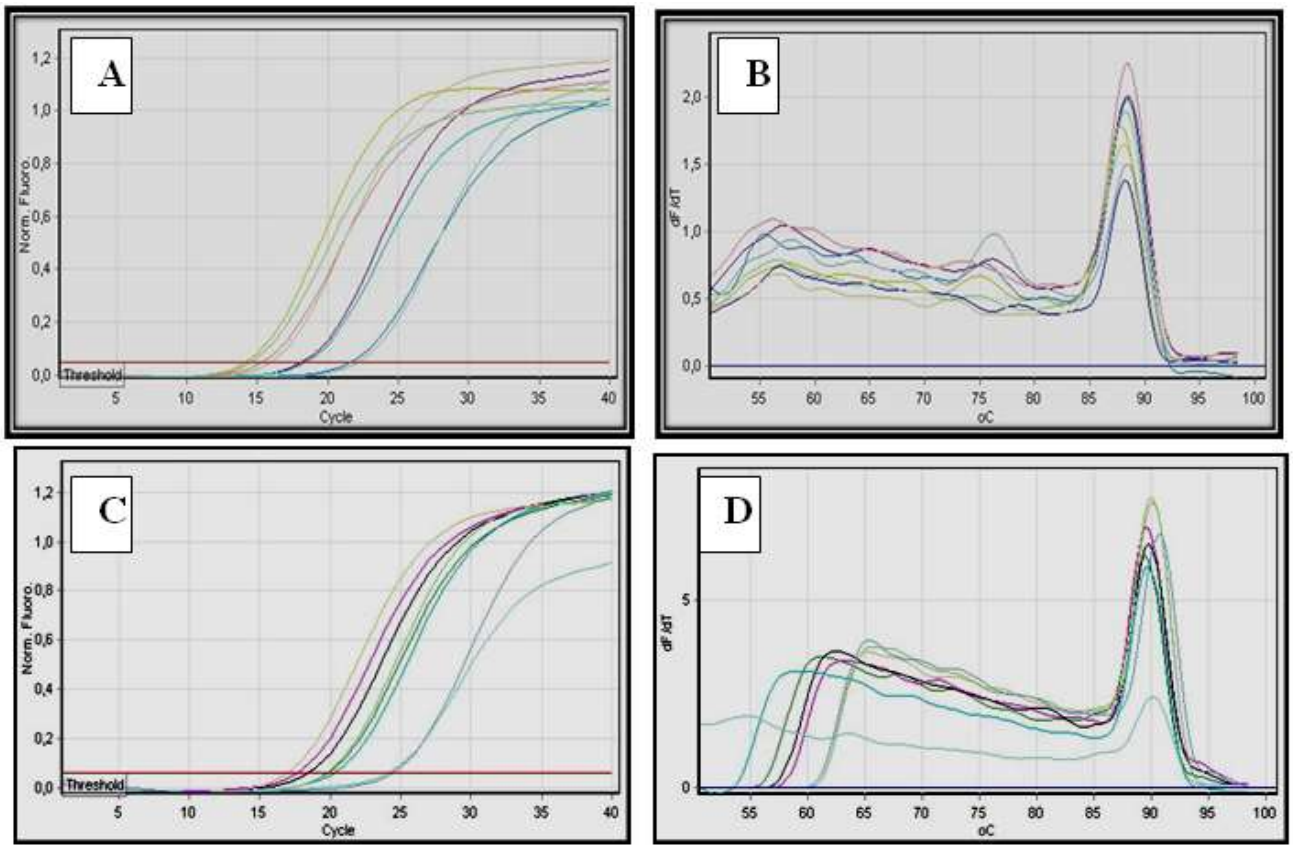

Figure 3-9: The amplification plots and Melting temperature curve ranged from 85°C to 90°C of *CsuE* gene before and after treatment with synthesis iron oxide nanoparticles (Fe3O4 NPs)

Real time PCR Quantification of *16Sr*RNA Gene Expression

In the present study *16Sr*RNA is the (reference or internal control) gene was used. The range of Ct value of this gene in untreated with the synthesized iron oxide nanoparticles Fe3O4 NPs from (14.25 to 14.83) in all A.baumannii isolates, were we then treated with synthesis Fe_3O_4 NPs, the Ct value found not changing at high rang from (14.38 to 14.97). The statistical analysis shown non-significant difference was found in between of them isolates and between off before and after treatment, The pattern of amplification of the gene shown in Figures (3-10 A and B) respectively. The purpose of the reference gene is to normalize the PCRs for the amount of RNA added to the reverse transcription reactions. Standard housekeeping genes usually are sufficient as internal control genes [37].

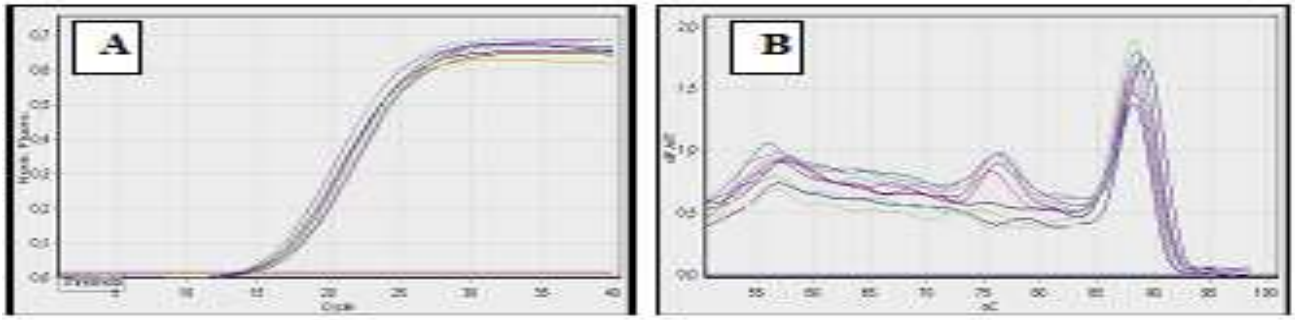

Figure 3-10: The amplification plots and Melting temperature curve ranged from 85°C to 90°C of housekeeping gene *16Sr*RNA

To determine whether *CsuE* expression is actually regulated, we performed qRT-PCR. Indeed biofilm formation in isolates with *CsuE* before treated with synthesized Fe3O4 NPs was significantly greater than after treated with synthesis nanoparticles ($p \leq 0.05$). In the current study, quantitative RT-PCR evaluate analyzed the mRNA expression of *CsuE* and internal control *16Sr*RNA genes by comparing before and after treatment with synthesized Fe_3O_4 NPs for each isolate, The calculation of gene expression fold change was done by using relative quantification from delta delta Ct value (ΔΔCt) [37].

This depends on normalization of Ct values calculating the ΔCt which is the difference between the mean Ct values of replica of *CsuE* cDNA amplification of each single case and that of the *16Sr*RNA. The alterations in gene expression levels can be visualized in Table (3-1), which was generated using the data-analysis tools. These Tables shows the mean of ΔCt (normalization Ct values) of each isolates for CsuE gene, depending on evaluate values for Ct of target genes with Ct for internal control. The results of ΔCT, ΔΔCT and 2-ΔΔCt showed that there was a significant difference ($P<0.05$) in the values between the different studied isolates, this difference according to the source of isolated. To calculate the folds of gene expression of *CsuE* gene in relation to the house keeping gene. Genes that showed statistically significant for the result of 2-ΔΔCt values for the isolates ranged determined from (0.059 to 0.279) for *CsuE* gene. These results indicate a significantly decrease expression of biofilm formation after treated with Fe_3O_4 NPs that shown in these Table. These results are consistent given that treated with Fe3O4 NPs causes the growth rate of the bacteria to decrease and decrease genes expressed.

The RT-PCR gene expression study indicated that a number of the genes within the bacterium were up-regulated at physiological biofilm. The importance of the *CsuE* gene in *A.baumannii* biofilm formation has been well established (6).Several previous researchers from studies about this bacterium and correlation with adherence and biofilm formation. Variation in the expression of factors involved in these pathways may account for the different capacity of bacterial strains to form biofilms and therefore to colonize or infect the host environment [38].

Table 3-1: Fold of gene expression of *CsuE* gene depending on ΔΔCt method

No. of isolates	Treatment	Ct CsuE of Target gene	Ct of reference 16SrRNA	ΔCt Target (Ct CsuE - Ct internal control	ΔΔCt	2-ΔΔCt Fold of gene expression
Ab 1	Untreated	14.56	14.83	- 0.27	3.01	0.124
	Treated	17.70	14.96	2.74		
Ab 2	Untreated	15.54	14.72	0.87	4.08	0.059
	Treated	19.90	14.95	4.95		
Ab 3	Untreated	14.39	14.28	0.11	3.84	0.069
	Treated	18.53	14.58	3.95		
Ab 4	Untreated	15.93	14.61	1.35	3.47	0.090
	Treated	19.77	14.95	4.82		
Ab 5	Untreated	14.16	14.25	-0.09	2.45	0.183
	Treated	17.02	14.66	2.36		
Ab 5	Untreated	21.62	14.44	7.18	2.37	0.193
	Treated	24.20	14.65	9.55		

Ab 7	**Untreated**	**22.13**	**14.81**	**7.32**	**2.22**	**0.214**
	Treated	**24.51**	**14.97**	**9.54**		
Ab 8	**Untreated**	**18.24**	**14.45**	**3.79**	**1.84**	**0.279**
	Treated	**20.30**	**14.67**	**5.63**		
LSD value (P-value)		**---**	**---**	**---**	**---**	**0.117 * (0.044)**
*** (P<0.05).**						

References

1. WHO, World Health Organization ,Geneva (2017) WHO Publishes List of Bacteria for which New Antibiotics are Urgently Needed. http://www. who.int/mediacentre/news/releases/bacteria-antibiotics-needed/en.
2. Antunes LCS, Visca P, Towner KJ (2014) Acinetobacter baumannii: evolution of a global pathogen, Pathogens and Disease, 71(3): 292-301.
3. MAJ Ford, M Lannan, Daniel KO' conor, Cadet USMA, Joseph C Broderick, Cadet USMA (2017) Evaluation of Virulence Gene Expression Patterns in Acinetobacter baumannii Using Quantitative Real-Time Polymerase Chain Reaction Array. Military Medicine, 181.
4. Lee J, Kim Y, Ryu SY, Cho MH, Lee J (2014) Resveratrol oligomers inhibit biofilm formation of Escherichia coli 0157: H7 and Pseudomonas aeruginosa. J. Nat. Prod., 77(1): 168-172.
5. Moghadam Solmaz Ohadian, Mohammad Reza Pourmand, Farzaneh Aminharati (2014) Biofilm formation and antimicrobial resistance in methicillin -resistant Staphylococcus aureus isolated from burn patients, Iran. J. Infect Dev. Ctries., 8(12):1511-1517.
6. Tomaras AP, Dorsey CW, Edelmann RE, Actis LA (2008) Attachment to and biofilm formation on abiotic surfaces by Acinetobacter baumannii: involvement of a novel chaperone-usher pili assembly system. Microbiology, 149(12): 3473-84.
7. De Breij, A Dijkshoorn, L Lagendijk, E van der Meer, J Koster, A Bloemberg, G Woterbeek, R van den, Broek P, Nibbering P (2010) Do bio film formation and interactions with human cells explain the clinical success of Acinetobacter baumannii PloS One, 5: 107-132.
8. Sahl Jason W, Gillece John D, James M Schupp, Victor G Waddell, Elizabeth M Driebe, David M Engelthaler, Paul Keim (2013) Evolution of a Pathogen: A Comparative Genomics Analysis Identifies a Genetic Pathway to Pathogenesis in Acinetobacter. PLOS. https://doi.org/10.1371/journal.pone.0054287.
9. Ramasamy M, Lee J (2016) Recent nanotechnology approaches for prevention and treatment of bioflm-associated infections on medical devices. Bio Med Research International, 1: 1-17.
10. Boisseau P, Loubaton B (2011) Nanomedicine, nanotechnology in medicine. Comptes Rendus Physique, 12: 620-636.
11. Ansari MA, Khan HM, Khan AA, Cameotra SS, Alzohairy MA (2015) Anti-biofilm efficacy of silver nanoparticles against MRSA and MRSE isolated from wounds in a tertiary care hospital. Indian Journal of Medical Microbiology, 33: 101-109.
12. Arias Yesica Flores, Gabriela Vázquez-Victorio, Raul Ortega-Zempoalteca, Ulises Acevedo-Salas, Souad Ammar, Raul Valenzuela. (2018) Magnetic phase transitions in ferrite nanoparticles characterized by electron spin resonance. Journal of Applied Physics 117, 17A503; doi: 10.1063/1.4916935 View online: http://dx.doi.org/10.1063/1.4916935.
13. Wang B, Wei Q, Qu S (2013) Synthesis and characterization of uniform and crystalline magnetite nanoparticles via oxidation-precipitation and modified co-precipitation methods". Int. J. Electrochem. Sci., 8: 3786-3793.
14. Meshram Lalit; Kumar, Patidar Rakesh; Mayuri,Khare; Swati, Bagde; N.,Sahare Keeritisheel and Vinod, Singh (2012) Comparative analysis between biofilm formation of commensal and pathogenic Escherichia coli isolate. Asiatic Journal of Biotechnology Resources, 3(10):1441-1446.

15. Soares J (2014) Optical materials characterization Advanced Materials Spectrometry. Analytical Chemistry, 84: 636–668.

16. Tsuji K, Nakano K, Takahashi Y, Hayashi K, Ro C-U (2012) X-ray. The Journal of Infectious Diseases, 215 (l-1): 15 S52–S57 https://doi.org/10.1093/infdis/jiw529.

17. Cullity BD, Stock SR (2001) Elements of x-ray diffraction, Pearson education, 3rd edition, published by Prentice Hall, 558.

18. Magonov SN, Elings V, Whangbo MH (2013) Phase imaging and stiffness in tapping-mode atomic force microscopy. Surf. Sci., 375: 385-391.

19. Hall JP, dobrovolskaia MA, Patri AK, MaNeil SE (2007) Characterization of nanoparticles for therapeutic. Nanomedicine (London).

20. CLSI, Clinical and Laboratory Standards Institute (2013) Performance Standards for Antimicrobial Susceptibility Testing; Twenty-Third Informational Supplement, 33 (1): M100-S23.

21. Chao Wei, Sheng-Nan, Zhu Zan-Zan, Hou Yang-Long, Subbu S Venkatramana, Xu Zhi-Chuan (2012) Magnetic iron oxide nanoparticles: Synthesis and surface coating techniques for biomedical applications. Chin. Phys. B., 23(3): 037503. DOI: 10.1088/1674-1056/23/3/037503

22. Idalina Machado Joana Graça Hélder Lopes; Susana Lopes and Maria O. Pereira (2013) Antimicrobial Pressure of Ciprofloxacin and Gentamicin on Biofilm Development by an Endoscope-Isolated Pseudomonas aeruginosa. J. Biotechnology. Vol. Article ID 178646, 10.

21. Gitanjali Kailas Badave, Kulkarni Dhananjay (2015) Biofilm Producing Multidrug Resistant Acinetobacter Baumannii: An Emerging Challenge. Journal of Clinical and Diagnostic Research, 9(1): DC08-DC10.

22. Namasivayam SKR, Preethi M, Bharani ARS, Robin G, Latha B (2013) Biofilm Inhibitory Effect of Nanoparticles coated catheter against Staphylococcus aureus and Evaluation of its Synergistic Effects with Antibiotics. Inte. J. Bio. Pharm. Res., 3: 259-265.

23. Skurikhina Yu, Ibragimova TD, LA Skurikhina, VB Turkutyukov (2016) Molecular Epidemiological Analysis of Acinetobacter baumannii Strains Isolated in Patients with Burn Injury. clinical medicine, CTM 8 (1) DOI: 10.17691/stm2016.8.1.18.

24. Higgins PG, Wisplinghoff H, Stefanik D, Seifert H (2004) Selection of topisomerase mutations and over expression of adeB mRNA transcripts during an outbreak of Acinetobacter baumannii. J. Antimicrob. Chemother., 54: 821-823.

25. Schmittgen TD, Lee EJ, Jiang J, Sarkar A, Yang L, Elton TS, Chen C (2008) Real-time PCR quantification of precursor and mature micro RNA. Methods, 44: 31-8.

26. Urdan TC (2005) Statistics In Plain English, 2nd ed. Lawrence Erlbaum Associates, London, 130-143.

27. El-Sigeny Samia M, Abou Taleb, Manal F (2015) Synthesis, Characterization, and Application of Dendrimer Modified Magnetite Nanoparticles as Antimicrobial Agent. Life Science Journal, 12 (6).

28. Pal S, Tak YK, Song JM (2007) Does the antibacterial activity of silver nanoparticles depend on the shape of the nanoparticle? A study of the Gram-negative bacterium Escherichia coli. Applied and Environmental Microbiology, 73: 1712-1720.

29. Zhang Y, Shareena Dasari, TP Deng, H Yu H (2015) Antimicrobial Activity of Gold Nanoparticles and Ionic Gold. Journal of Environmental Science and Health.

30. Balamurughan MG, Mohanraj S, Kodhaiyolii S, Pugalenthi V (2014) Ocimum sanctum leaf extract mediated green synthesis of iron oxide nanoparticles: spectroscopic and microscopic studies. J. of Chemical and Pharmaceutical Sci., 4: 201-204.

31. D Chicea, E Indrea, CM Cretu (2012) Assessing Fe3O4 nanoparticle size by DLS, XRD and AFM. journal of optoelectronced and Advanced Materials, 14 (5-6): 460-466.

32. Nayamadi A Mahmoodabadi, A Kompany, M Mashreghi (2018). Characterization, antibacterial and cytotoxicity studies of graphene-Fe_3O_4 nanocomposites and Fe_3O_4 nanoparticles synthesized by a facile solvothermal method. Materials Chemistry and Physics, 213 (1): 285-294.

33. Parsek MR, Singh PK (2003) Bacterial biofilms: an emerging link to disease pathogenesis. Annu Rev Microbiol. 57:677-701.DOI:10.1146/annurev.micro.57.030502.090720.

34. SharmalP S Rana, KC Barick, C Kumar, H G Salunke, PA Hassan (2015) Biocompatible phosphate anchored Fe3O4 nanocarriers for drug delivery and hyperthermia New J. Chem., 5500-5508.

35. Schmittgen TD, Livak KJ Analyzing (2008) Real-time PCR data by the comparative C(T) method. Nature Protocol 3(6): 1101-1108.DOI: 10. 1038/nprot. 2008. 73.

36. Bahador Abbas, Zahra Farshadzadeh, RezaRaoofian, MasoumehMokhtaran, Babak ourakbari and Farhad B. Hashemi. (2018) .Association of virulence gene expression with colistin-resistance in Acinetobacter baumannii: analysis of genotype, antimicrobial susceptibility, and biofilm formation. Annals of Clinical Microbiology and Antimicrobials. 17:24. https:// doi.org/ 10.1186/s12941-018-0277-6.

